energies

MDPI

Article

Design Consideration of Bidirectional Wireless Power Transfer and Full-Duplex Communication System via a Shared Inductive Channel

Jie Wu [1,*], Weihao Kong [1], Pengfei Gao [1], Nan Jin [1], Jitao Zhang [1], Jiagui Tao [2] and Václav Snášel [3,*]

[1] School of Electrical and Information Engineering, Zhengzhou University of Light Industry, Zhengzhou 450002, China; kongweihao@zzuli.edu.cn (W.K.); 2019036@zzuli.edu.cn (P.G.); jinnan@zzuli.edu.cn (N.J.); zhangjitao@zzuli.edu.cn (J.Z.)

[2] State Grid of Jiangsu Electric Power Co., Ltd., Nanjing 210024, China; taojiagui@sgcc.com.cn

[3] Faculty of Electrical Engineering and Computer Science, VŠB-Technical University of Ostrava, 70032 Poruba-Ostrava, Czech Republic

* Correspondence: wujie@zzuli.edu.cn (J.W.); vaclav.snasel@vsb.cz (V.S.)

Citation: Wu, J.; Kong, W.; Gao, P.; Jin, N.; Zhang, J.; Tao, J.; Snášel, V. Design Consideration of Bidirectional Wireless Power Transfer and Full-Duplex Communication System via a Shared Inductive Channel. *Energies* **2021**, *14*, 4918. http://doi.org/10.3390/en14164918

Academic Editor: Nicu Bizon

Received: 7 June 2021
Accepted: 7 August 2021
Published: 11 August 2021

Abstract: Communication between the primary and secondary sides is pivotal to the wireless power transfer (WPT) system. The system control commands and feedback information need simultaneous wireless information and power transfer (SWIPT). In this paper, a FSK-based SWIPT system with full-duplex communication via a shared channel is provided. Considering the complexity of the coupling relationship in this kind of full-duplex SWIPT system, this paper proposes an analysis method based on the transmission channel, studies the crosstalk between the power channel and the information channel, and between the forward and reverse transfer of information. A design method of full-duplex communication SWIPT system based on shared coupling channels is provided. A 60 W SWIPT prototype with a full-duplex communication rate of 20 kbps is built to verify the proposed method.

Keywords: bidirectional power transmission; crosstalk; FSK; full-duplex information transfer; information transfer channel gain; SWIPT

1. Introduction

Based on convenience and safety, wireless power transfer (WPT) technology has been developed rapidly in the field of electric vehicles [1–3], urban rail transit [4], motor control [5,6], LED [7], and so on. Along with the development and optimization of new devices [8,9], topology and coil structure [10,11], the performance of WPT system has greatly improved.

For WPT system, bidirectional power transfer can improve the energy utilization and increase the interaction between the power grid and electrical equipment, such as vehicle-to-grid (V2G), autonomous underwater vehicle, implantable medical devices [12–14]. However, for the industrial applications, it is necessary to monitor the actual working state of the devices, and the information transfer needed [15]. Reliable communication between the primary and secondary side plays a critical role in wireless transmission systems. If communication between the two sides is provided, it is easier to implement system requirements in specific applications, such as output voltage feedback control, load detection and status monitoring.

Varshney [16] proposed a simultaneous wireless information and power transfer technology (SWIPT) for the first time, giving a trade-off method between signal capacity and energy efficiency suitable for discrete channels and Gaussian channels. Subsequently, Grover et al. [17] proposed a circuit model that uses a coupled inductance circuit to achieve the simultaneous transmission of short-range wireless information and energy, and applied the water injection algorithm to the SWIPT system to achieve the optimal distribution of information energy power. In view of the fact that the actual hardware may not be able to demodulate information and receive energy at the same time, Clerckx et al. [18] proposed a dynamic power allocation method, and on this basis, proposed a separate and integrated receiver. The authors in [19–21] further studied the receiver models suitable for SWIPT, including models such as time allocation and power allocation. Power and information are transmitted in different time period, which reduces the power transmission time to a certain extent and affects the power transmission performance. In addition, in order to ensure the reliability of power transmission, the time allocated for signal transmission is relatively short, which mainly limits the signal transmission rate.

There are many ways to achieve information transmission in SWIPT system, including radio frequency (RF), dual channel mode, and shared channel mode. For Bluetooth, WiFi, NRF2401 and other RF system, the structures are simple and the transmission speed is stable. However, the reliability and stability of the system may decline in complex electromagnetic environment [22]. The dual-channel technology employs additional information transmission coils. Due to the coupling between the coils, system analysis, and design become complicated. Shared channel technology has the advantages of high integration, stable and reliable information transmission [23–25].

In shared channel technology, signal transmission modes can be divided into power modulation mode and carrier modulation mode [26–28]. For the power modulation mode, the information transfer can be realized by the voltage regulation, frequency modulation or tuning. In the SWIPT system, adding a voltage regulation circuit in the main circuit, the information is modulated on the power carrier by changing the input voltage [29]. The frequency modulation method changes inverter operating frequency that makes the system be in a resonant or non-resonant state. The information is obtained by detecting the voltage amplitude envelope [30,31]. The tuning method affects the current by changing the compensation parameters of the circuit, thereby achieving information transfer [32]. These modulation methods have simple structures and principles, so they are easy to implement. However, the information transfer data are limited by the power transfer rate. Meanwhile, the power transfer quality and efficiency are affected by changing the circuit parameters and operating frequency.

For the carrier modulation mode, the baseband signal spectrum is broadened by sinusoidal carrier modulation techniques. It facilitates the transmission of signals on the channel. Literature [33] proposed a SWIPT system, based on FD, and provided the circuit model and measurement results. Among them, the carrier frequency of power and information is 22.4 kHz and 1.67 MH, respectively. In order to reduce the influence of the information transfer frequency on the power transfer efficiency, the information transfer frequency is at least an order of magnitude higher than the power transfer frequency. In [34], information and power are simultaneously transmitted in a single inductive link by using different carrier frequencies. Taking forward transmission as an example, the modulated high-frequency data carrier is injected into the primary side of the system. Then, the superimposed signal, composed of the power carrier and the information carrier is transmitted to the secondary side, and finally the data carrier in the superimposed signal is extracted by the demodulation module on the secondary side. This method is essentially a frequency division multiplexing (FDM) technology. Literature [35] proposed a full-duplex communication by modulating dual carrier using quadrature phase shift keying. In [36], frequency shift keying is used to achieve full-duplex communication through partially coupled coils. However, complex modulation and demodulation methods may limit their application space.

Although this transmission method has many advantages, there are also challenges. In full-duplex operation, the forward transmission signal and the reverse transmission signal circulate in the circuit simultaneously, and the signal is injected into the power loop, that is, there are three frequencies in the system at the same time, so there are inevitable interferences on the three coupling channels, such as the forward/reverse information transmission channel and the power transmission channel. A huge challenge to system design is posed when these complex coupling relationships are intertwined.

Taking into account the complexity of the coupling relationship in the full-duplex communication SWIPT system with a shared coupling channel, this paper proposes an analysis method based on the transmission channel, and studies the crosstalk between the power channel and the information channel, and between the forward and reverse transfer of information. A design method of full-duplex communication SWIPT system based on shared coupling channels is provided. Finally, the effectiveness of the proposed SWIPT method is verified by the experiment.

2. System Overview and Power Channel Analysis

The block diagram of the proposed SWIPT system is shown in Figure 1a. The system is divided into the primary and secondary side. Both sides are supplied by the DC power. The inductive link bridges the primary and the secondary sides. The information is injected into the bidirectional power transfer loop through the signal coupling transformer at both sides, which can achieve the full-duplex transmission of the signal.

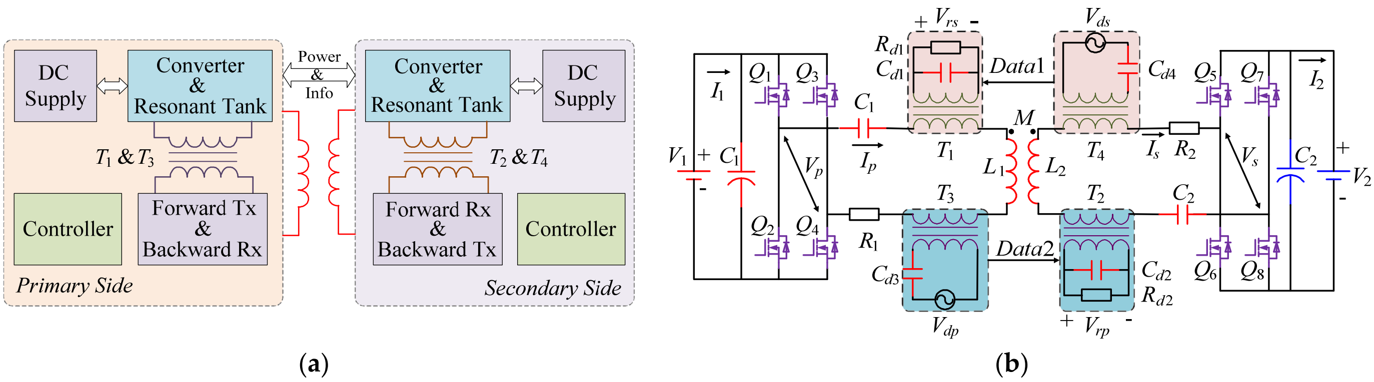

Figure 1. The bi-directional SWIPT system. (**a**) Block diagram. (**b**) Schematic diagram.

The schematic diagram of the proposed SWIPT system is shown in Figure 1b. The primary side and secondary side adopt the active bridges for bidirectional power transfer. V_1 and V_2 are the DC power supply in the primary and secondary side, respectively. The compensation structure of the circuit employs series compensation. Inductance and capacitance are connected in series in the circuit. As I_p and I_s are high-frequency currents, in order to reduce the AC resistance on the coil, the inductor coil uses multiple Litz wires. Four coupled transformers (T_1~T_4) are combined to form a signal modulation section and signal receiving section to complete the transmission and reception of signals.

The combination of the transformers T_1 and T_4 is employed in backward information transfer. T_3 and T_2 are applied for forward information transfer. The forward and the backward information transfer frequency are 1.7 MHz and 1 MHz, respectively. Besides, V_{dp} and V_{ds} are high frequency sources of forward information and backward information transfer, respectively. V_{rp} and V_{rs} are the voltage of forward and backward information pick-up resistances, respectively. As the injected signals frequencies are different, the transmitting circuit and the receiver circuit parameters are different and this structure can realize forward and backward information transfer dependently.

In order to achieve bidirectional power transmission, the SWIPT system adopts dual active full bridges. The power transfer size and direction is controlled by the three phase-shift, α, β, and ϕ, where α and β are half of the inter-bridge phase shift angle of the primary side and secondary sides, respectively; ϕ is the phase shift angle between the primary full-bridge arms and the secondary full-bridge arms, and it can adjust power transmission direction.

Figure 2 shows the eight switches control signals of the dual active bridges. S_1~S_4, S_5~S_8 are the primary side and secondary side control signals, respectively. V_p and V_s are output three-level square wave voltage signals of the primary side and secondary side.

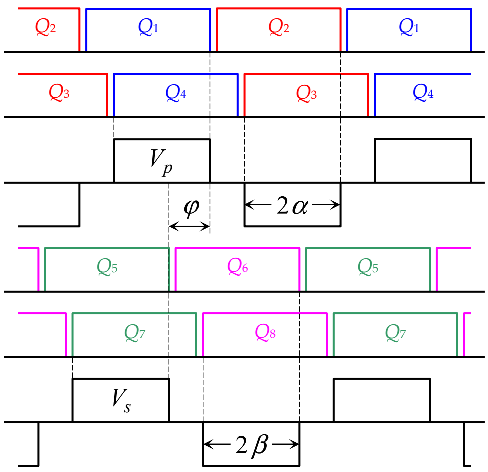

Figure 2. The timing diagram of phase shift control signals.

The equivalent circuit model of the proposed SWIPT system is presented in Figure 3, where L_{T1}~L_{T4} are the equivalent inductance of the tightly coupled transformer. During power transfer, the impedance of the tightly coupled transformer inductor L_{T1}~L_{T4} are much smaller than the reflected impedance of information demodulation cells. V_p and V_s are the primary and secondary inverter output voltage. In order to simplify analysis, only the amplitude of fundamental frequency component is retained and higher harmonics are ignored. Then V_p and V_s are equivalent to:

$$V_p = \frac{2\sqrt{2}}{\pi} V_1 \sin\alpha, \ V_s = \frac{2\sqrt{2}}{\pi} V_2 \sin\beta. \tag{1}$$

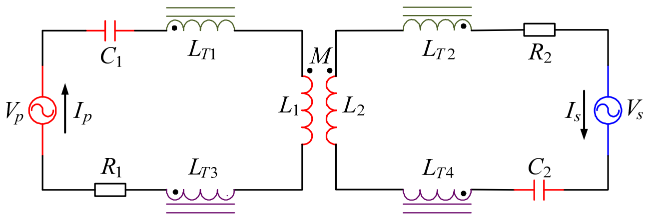

Figure 3. The schematic diagram of the SWIPT system equivalent circuit.

Define V_p as the reference voltage, so the expression of the V_p and V_s is:

$$\begin{cases} \dot{V}_p = V_p\angle 0^\circ \\ \dot{V}_s = V_s\angle\phi \end{cases}, \tag{2}$$

where ϕ is the phase shift angle generated between the primary side and the secondary side control signal. According to the Kirchhoff's theorem, the circuit equation is obtained.

$$\begin{bmatrix} Z_1 & -j\omega_p M \\ -j\omega_p M & Z_2 \end{bmatrix} \cdot \begin{bmatrix} I_p \\ I_s \end{bmatrix} = \begin{bmatrix} V_p \\ V_s \end{bmatrix}, \tag{3}$$

where

$$Z_1 = j\omega_p(L_1 + L_{T1} + L_{T3}) + \frac{1}{j\omega_p C_1} + R_1, \tag{4}$$

$$Z_2 = j\omega_p(L_2 + L_{T2} + L_{T4}) + \frac{1}{j\omega_p C_2} + R_2. \tag{5}$$

The power transfer frequency is necessary to work at the circuit resonance frequency. C_1 and C_2 compensate the inductance of the primary and secondary coils. The power resonant angular frequency ϖ_p is obtained from the inductance and compensation capacitance values in the circuit.

$$\omega_p = \frac{1}{\sqrt{(L_1 + L_{T1} + L_{T3})C_1}} = \frac{1}{\sqrt{(L_2 + L_{T2} + L_{T4})C_2}} \tag{6}$$

The active power P_1 and P_2 of the primary and secondary sides are

$$P_1 = \mathrm{Re}\{V_p \cdot I_p^*\} = \frac{R_2 V_p^2 + \omega_p M V_p V_s \sin\phi}{R_1 R_2 + \omega_p^2 M^2} \tag{7}$$

$$P_2 = \mathrm{Re}\{V_s \cdot I_s^*\} = \frac{-R_1 V_s^2 + \omega_p M V_p V_s \sin\phi}{R_1 R_2 + \omega_p^2 M^2} \tag{8}$$

According to the Equations (7) and (8), ignoring the resistances R_p and R_s, the secondary side output power P_{out} is obtained.

$$P_{out} \approx \frac{8}{\pi^2 \omega_p M} V_1 V_2 \sin\alpha \sin\beta \sin\phi \tag{9}$$

The range of α and β is [0, π]. The range of ϕ is [0, 2π]. Therefore, Equation (9) shows that the direction of the output power is determined by ϕ. The magnitude of the transmission power is affected by the phase shift angles α, β, and ϕ. The bidirectional power transfer can be realized by changing the phase shift angle ϕ.

Figure 4 shows the curve of output power with the phase shift angle ϕ. During a period cycle, in the interval $[0, \pi]$, sinϕ > 0, the output power is transmitted from the primary side to the secondary side; in the interval $[\pi, 2\pi]$, sinϕ < 0, the output power is transferred from the secondary side to the primary side. However, in order to ensure the maximum output power, the value of ϕ is chosen between $-\pi/2$ and $\pi/2$. In short, the working states of the proposed SWIPT system is decided by the values of α, β, and ϕ.

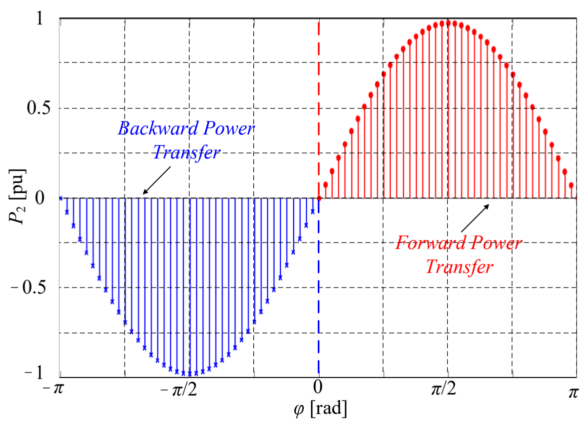

Figure 4. The output power with respect to phase shift angle ϕ.

3. Signal Path Modeling and Analysis

In this system, information communication is implemented through magnetic induction communication technology based on the FSK control method. The carrier frequencies of forward and backward information transfer are 1.7 MHz and 1 MHz, respectively. It is obvious that the system information carrier frequencies are much larger than the power carrier frequency. According to superposition theorem, information transmission and power transmission are discussed separately. Therefore, when high frequency information is being transferred, the low frequency loop can be regarded as a short circuit to simplify the analysis of the information coupling loop. This section separately analyzes forward and backward information transmission.

3.1. Forward Information Transfer Channel Analysis

The circuit model of the forward signal transmission channel is shown in Figure 5a. For the forward information transfer, the information is injected into the power carrier on the primary side. The information is emitted by the high-frequency source V_{dp} and amplified by the *LC* resonant circuit. Then, the power and the information carrier transmit through the common inductive link from the primary side to the secondary side. On the receiver side, the *LC* circuit is tuned in the forward information transfer frequency to select and amplify the high-frequency carrier signal while attenuating the strength of other carriers.

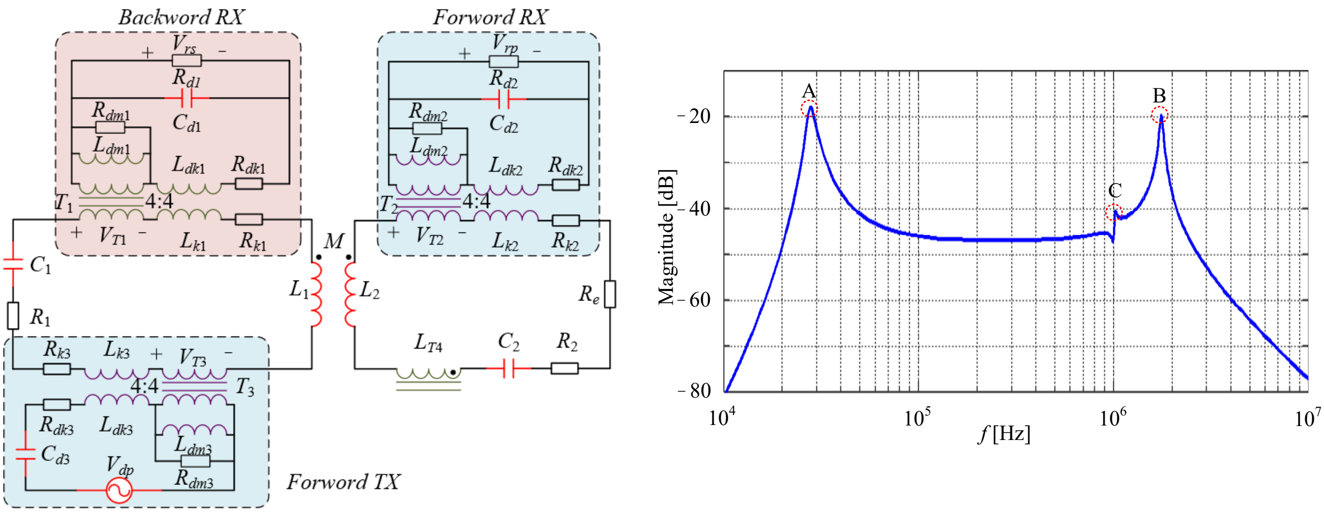

(**a**) (**b**)

Figure 5. Forward information transfer channel. (**a**) Simplified schematic of the forward transmission channel. (**b**) Bode plot of the forward information transmission.

In order to enhance the forward and backward information transmission and the strength of reception, the transmitting and receiving modules are resonant at the information carrier frequency. The angular frequencies of the forward or backward information transmission are ω_{dp} and ω_{ds}, respectively.

The equivalent circuit of the signal coupling transformer is shown in Figure 5a, where R_{md1}~R_{md4} are the core loss resistance, L_{md1}~L_{md4} are the mutual inductance, L_{k1}~L_{k4} and L_{dk1}~L_{dk4} are the leakage inductance of the four tightly coupled transformers, R_{k1}~R_{k4} and R_{kd1}~R_{kd4} are leakage resistance. According to Figure 5a, the equivalent impedance of the signal receiver network is

$$Z_{T1}(\omega) = \frac{1}{\frac{1}{j\omega L_{md1}} + \frac{1}{R_{md1}} + \frac{1}{j\omega L_{kd1} + R_{kd1} + 1/(j\omega C_{d1} + 1/R_{d1})}} \tag{10}$$

$$Z_{T2}(\omega) = \frac{1}{\frac{1}{j\omega L_{md2}} + \frac{1}{R_{md2}} + \frac{1}{j\omega L_{kd2} + R_{kd2} + 1/(j\omega C_{d2} + 1/R_{d2})}} \tag{11}$$

The coupled inductance at transmitter side is ignored because its inductance is much smaller than the coil inductance. Thus, the secondary side impedance $Z_s(\varpi)$ is:

$$Z_s(\omega) = j\omega L_2 + \frac{1}{j\omega C_2} + R_2 + Z_{T2}(\omega) + j\omega L_{k2} + R_{k2} + j\omega L_{T4} \tag{12}$$

The impedance of the secondary side reflected in the primary side is:

$$Z_{rs}(\omega) = \frac{\omega^2 M^2}{Z_s(\omega)} \tag{13}$$

The primary side impedance is equivalent to:

$$Z_p(\omega) = j\omega L_1 + \frac{1}{j\omega C_1} + R_1 + j\omega L_{k1} + R_{k1} + Z_{T1}(\omega) + Z_{rs}(\omega) \tag{14}$$

The gain of the information demodulation voltage at the secondary side is:

$$G_{T2}(\omega) = \frac{V_{rp}}{V_{T2}} = \frac{1/(j\omega C_{d2} + 1/R_{d2})}{j\omega L_{kd2} + R_{kd2} + 1/(j\omega C_{d2} + 1/R_{d2})} \tag{15}$$

The gain of the tight coupled transform T_3 is:

$$G_{T3}(\omega) = \frac{V_{T3}}{V_{dp}} = \frac{1/(1/j\omega L_{md3} + 1/R_{md3})}{j\omega L_{kd3} + R_{kd3} + \frac{1}{j\omega C_{d3}} + \frac{1}{1/j\omega L_{md3} + 1/R_{md3}}} \tag{16}$$

So the forward information transmission gain G_{fd} (ϖ) is:

$$G_{fd}(\omega) = \frac{V_{rp}}{V_{dp}} = \frac{Z_{T2}(\omega)}{Z_p(\omega)} \cdot \frac{j\omega M}{Z_s(\omega)} \cdot G_{T2}(\omega) \cdot G_{T3}(\omega) \tag{17}$$

The bode plot of different carrier frequencies G_{fd} (ϖ) is shown in Figure 5b. There exist three extreme points in this figure, where the low-frequency point A is the power carrier frequency and the higher gain frequency point B is the forward information carrier transmission frequency 1.7 MHz. Another extreme point C is the backward information transmission channel point.

3.2. Backward Information Transfer Channel Analysis

The signal backward transmission equivalent circuit is shown in Figure 6a. Backward transmission and forward transmission are considered symmetric structures. The backward signal transmission and forward signal transmission employ similar analysis methods. When analyzing backward information transmission, the reflected impedance of demodulation circuits on both sides cannot be ignored, but the reflected impedance of the primary modulation circuit will be substituted by L_{T3}.

According to the equivalent circuit impedance analysis, the primary equivalent impedance Z_{ps} is:

$$Z_{ps}(\omega) = j\omega L_1 + \frac{1}{j\omega C_1} + R_1 + j\omega L_{T3} + j\omega L_{k1} + R_{k1} + Z_{T1}(\omega) \tag{18}$$

$Z_{rp}(\varpi)$ is the reflected impedance of the primary side to the secondary side:

$$Z_{rp}(\omega) = \frac{\omega^2 M^2}{Z_{ps}(\omega)} \tag{19}$$

The secondary side equivalent impedance Z_{ss} is:

$$Z_{ss}(\omega) = j\omega L_2 + \frac{1}{j\omega C_2} + R_2 + j\omega L_{k2} + R_{k2} + Z_{T2}(\omega) + Z_{rp}(\omega) \tag{20}$$

The gain of backward information demodulation cell is:

$$G_{T1}(\omega) = \frac{V_{rs}}{V_{T1}} = \frac{1/(j\omega C_{d1} + 1/R_{d1})}{j\omega L_{kd1} + R_{kd1} + 1/(j\omega C_{d1} + 1/R_{d1})} \tag{21}$$

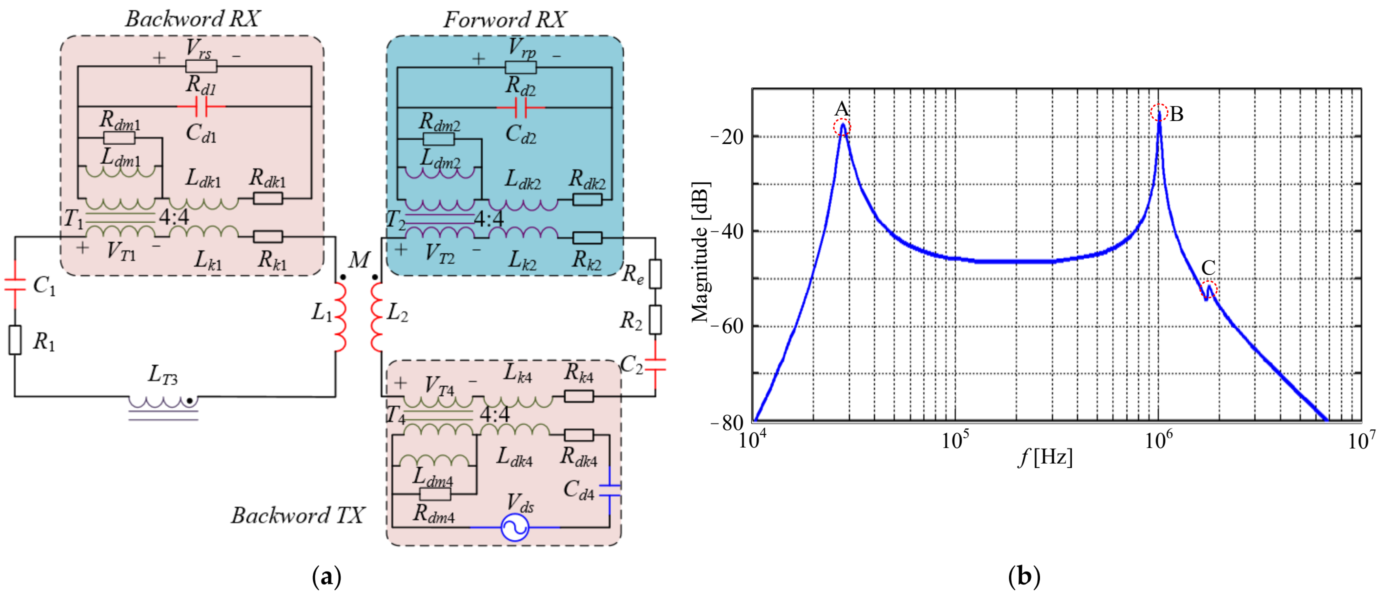

Figure 6. Backward information transfer channel. (**a**) Simplified schematic of the backward transmission channel. (**b**) Bode diagram of the backward information transmission.

The transfer function of the tight coupled transform T_4 is:

$$G_{T4}(\omega) = \frac{V_{T4}}{V_{ds}} = \frac{1/(1/j\omega L_{md4} + 1/R_{md4})}{j\omega L_{kd4} + R_{kd4} + \frac{1}{j\omega C_{d4}} + \frac{1}{\frac{1}{j\omega L_{md4}} + \frac{1}{R_{md4}}}} \tag{22}$$

So the backward information transmission gain is:

$$G_{bd}(\omega) = \frac{V_{rs}}{V_{ds}} = \frac{Z_{T1}(\omega)}{Z_{ss}(\omega)} \cdot \frac{j\omega M}{Z_p(\omega)} \cdot G_{T1}(\omega) \cdot G_{T4}(\omega) \tag{23}$$

The backward information transmission gain $G_{bd}(\varpi)$ is shown in Figure 6b. Obviously, there are also three extreme points. The lower frequency point A is the power carrier frequency. The frequencies of other two extreme points B and C are the forward and backward information transmission carrier frequencies, respectively. As shown in Figure 6b, the backward information transmission carrier frequency is 1 MHz. The transmission gain of point B is larger than that of point C, which is advantageous to backward information transmission and demodulation.

4. Crosstalk Analysis

In the proposed SWIPT system, the origin of information interference is mainly generated by the power carrier and two different frequencies information carriers. As shown in Figure 7, the proposed SWIPT system can be equivalent to a six-port network. The power is transferred from port "V_p" to "V_s". The normal forward information is delivered from "Forward TX" to "Forward RX". The normal backward information transmission channel goes from port "Backward TX" to "Backward RX".

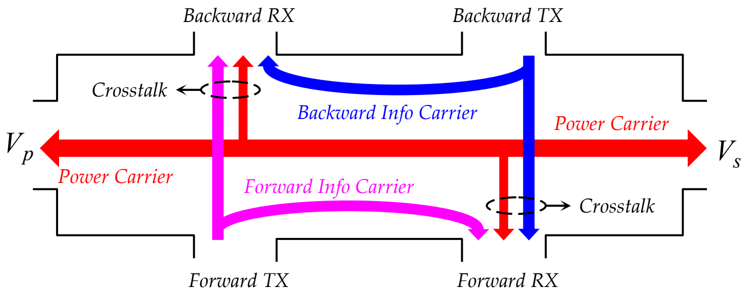

Figure 7. Six-port network of the wireless information and power transfer system.

Because the signal coupled coils are connected in series in the main circuit, some low-frequency voltage waveforms are also induced on the coupled coil during power transmission, so the power carrier is the main noise during signal transmission, such as "V_p" to "Backward RX" and "V_s" to "Forward RX".

At the same time, when the information is transmitted in both directions, the signal receiving coupling coils is not only affected by the power carrier but also disturbed by another signal source, for example, "forward TX" to "Backward RX" and "Backward TX" to "Forward RX".

To sum up, for the signal receiver cells, there are two main types of crosstalk source, one is the power carrier and the other is the high frequency signal source at the same side. Therefore, the system needs to establish two kinds of crosstalk equivalent models. Besides, it is beneficial to the design of the signal demodulation circuit by analyzing the influence of crosstalk on signal receiving port. The analysis of these two situations is as follows.

4.1. Crosstalk between Power Transfer and Information Transfer

The equivalent circuit models of crosstalk interference between power transfer and information transfer are shown in Figure 8. When analyzing the crosstalk form power loop to information loop, the magnetic coupling interface on the signal modulation and demodulation modules are equivalent to the inductance L_{T1}~L_{T4}. R_{ep} and R_{es} are the equivalent implement of the full-bridge and DC source in the primary side and the secondary side, respectively.

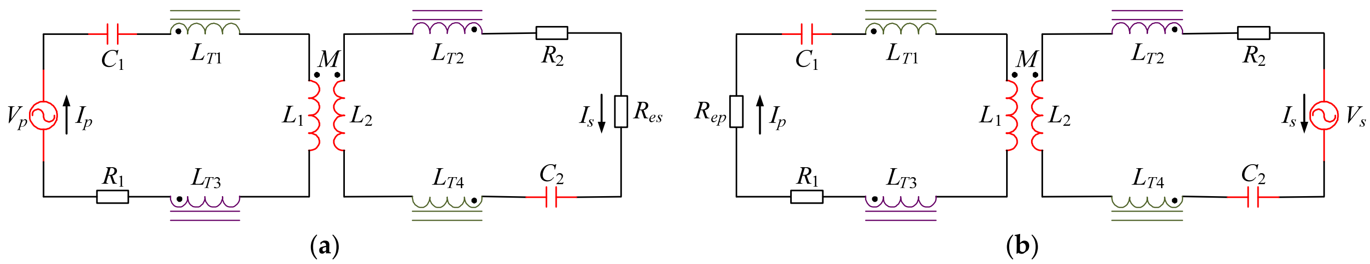

Figure 8. Equivalent circuit of crosstalk interference between power transfer and information transfer: (**a**) Simplified schematic of forward power transmission channel. (**b**) Simplified schematic of backward power transmission channel.

As shown in the Figure 8, the structures of circuit topologies are symmetrical. The noise interference of forward power transmission to the information loop signal transmission is analyzed. The noise transfer function $G_{NT1}(\omega)$ and $G_{NT2}(\omega)$ of signal receiving cells in the primary side and the secondary side are:

$$G_{NT1}(\omega_p) = \frac{V_{LT1}(\omega_p)}{V_p} = \frac{j\omega_p L_{T1}}{Z_p(\omega_p)} \tag{24}$$

$$G_{NT2}(\omega_p) = \frac{V_{T2}(\omega_p)}{V_p} = \frac{j\omega_p M}{Z_p} \cdot \frac{j\omega_p L_{T2}}{Z_s} \tag{25}$$

Define $L_1 + L_{T1} + L_{T3} = L_m$ and $L_2 + L_{T2} + L_{T4} = L_n$, at this time, the voltages in the impedance of the primary and secondary loop coils are:

$$V_{Lm}(\omega_p) = \frac{j\omega_p L_1 + Z_{rs}(\omega_p)}{Z_p(\omega_p)} V_p(\omega_p) \tag{26}$$

$$V_{Ln}(\omega_p) = \frac{j\omega_p M}{Z_p(\omega_p)} \cdot \frac{j\omega_p L_n + R_2}{Z_s(\omega_p)} V_p(\omega_p) \tag{27}$$

Since the coupling coefficient of the power coil is small, the reflected impedance $Z_{rs}(\omega_p)$ can be approximately ignored. From (24) and (26), it draws a conclusion:

$$\frac{V_{T1}(\omega_p)}{V_{Lm}(\omega_p)} \approx \frac{L_{T1}}{L_m} \tag{28}$$

Similarly, the internal resistance R_2 of the power coil on the secondary circuit is small, which has little influence on crosstalk analysis, so that it can be ignored. The voltage of power coil on the pickup side is:

$$\frac{V_{T2}(\omega_p)}{V_{Ln}(\omega_p)} \approx \frac{L_{T2}}{L_n} \tag{29}$$

According to Equations (28) and (29), the smaller the signal coupling inductance is, the lower the crosstalk interference is. Therefore, in the signal transmission process, the crosstalk interference generated from the power carrier can be weakened by reducing the coupled inductance.

4.2. Analysis of Signal-to-Noise Ratio between Forward and Backward Information Transfer

In order to analyze the influence of the relationship between noise interference and information transmission, the ratio between signal power and noise is defined as the signal-to-noise ratio. Taking the forward transmission of information as an example, then we get:

$$SNR = 20\log\frac{V_R\ (\omega_d,\ V_d)}{V_R\ (\omega_p,\ V_1)} \tag{30}$$

The signal carrier amplitude of the secondary side information receiving end is $V_R(\varpi_d,V_d)$, where ϖ_d is the information transmission angular frequency. According to the information forward transmission channel gain G_{fd}, we have:

$$V_R\ (\omega_d,\ V_d) = \frac{V_{dp}}{1 + \frac{L_1}{L_2}\frac{R_d/\omega L_{T1} - \omega C_d R_d + j}{R_d/\omega L_{T1}}} = \frac{V_{dp}}{1 + \frac{L_1}{L_2}\frac{Q - \omega C_d R_d + j}{Q}} \tag{31}$$

where Q is the quality factor of the LC resonant circuit when the signal is accepted.

According to the transfer functions G_{NT1} and G_{NT2} of the power carrier to the transmitting end and the receiving end of the information forward transmission process, the power carrier amplitude of the signal receiving end is $V_r(\omega_p,V_o)$, where ω_p is the angular frequency of electric energy transmission. According to Formulas (24) and (25).

$$V_r\ (\omega_p, V_1) = \frac{\omega^2 M V_1 L_{T1}}{R_2\ (R_e + R_d) + \omega^2 M^2} \tag{32}$$

Incorporating the above two formulas into *SNR*, the signal-to-noise ratio formula is:

$$SNR = 20\log\frac{V_d}{V_1} + 10\log\frac{L_1}{L_2} + 20\log\frac{K\left[R_2\left(R_{ep}+R_d\right)+\omega^2M^2\right]}{(1-K^2)\omega^2 M L_{T1}\left(1+\frac{L_1}{L_2}\frac{Q+j-\omega C_d R_d}{Q}\right)} \tag{33}$$

Among them, V_d is the voltage of the transmission source of the information forward transmission signal, and V_1 is the DC power supply of the power transmission loop. According to Formula (33), when the system coil and circuit parameters are determined, the signal-to-noise ratio of information transmission is related to the coil coupling coefficient K, the quality factor of the LC resonance circuit and the information transmission frequency. In order to improve the signal-to-noise ratio of signal transmission, the coil coupling coefficient K and quality factor Q can be improved. Therefore, when designing a signal transmission system, the system parameters should be fully and reasonably designed to reduce the system frequency transmission crosstalk and improve the signal-to-noise ratio, thereby reducing the bit error rate in the transmission, so that the signal demodulation module can successfully receive the transmitted signal and complete the information transmission.

4.3. Crosstalk between Forward and Backward Information Transfer

As shown in Figure 9, the process of bi-directional information transfer is not only influenced by crosstalk between information and power, but also interfered by the high-frequency signal source on the same side. According to the Section 3, $G_{fd}(\omega)$ and $G_{sd}(\omega)$ are the gain of forward and backward information transfer channel, respectively. Define $G_{fdc}(\omega)$ as the gain of the channel from "Backward TX" to "Forward RX" and define $G_{sdc}(\omega)$ as the gain of the channel from "Forward TX" to "Backward RX".

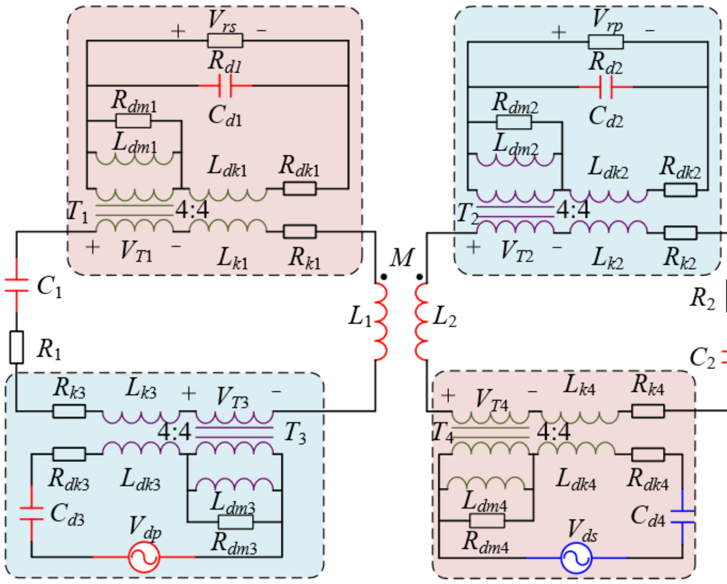

Figure 9. Equivalent circuit of crosstalk interference between forward information transfer and backward information transfer.

During the forward information transfer, the signal pick-up cell in the secondary side can not only receive the signal from the signal transmitter in the primary side, but also receive the signal from the signal transmitter in the secondary side.

Therefore, the crosstalk comes from the signal transmitter in the secondary side. The gain of the crosstalk $G_{fdc}(\omega)$ is:

$$G_{fdc}(\omega) = \frac{V_{rp}}{V_{ds}} = \frac{Z_{T2}(\omega)}{Z_{ss}(\omega)} \cdot G_{T2}(\omega) \cdot G_{T4}(\omega) \tag{34}$$

The bode plot of crosstalk $G_{fdc}(\varpi)$ is shown in Figure 10a. There are only two extreme points. Point A is the power carrier, point B and point C are the information transfer gain in ϖ_{ds} and ϖ_{dp}, respectively. However, point B is the gain of the channel from "Backward TX" to "Forward RX", called $G_{fdc}(\varpi_{ds})$. Comparing the gain of $G_{fd}(\varpi_{dp})$ and $G_{fdc}(\varpi_{ds})$, it is clear that $G_{fd}(\varpi_{dp})$ is greater than $G_{fdc}(\varpi_{ds})$. Therefore, during the process of forward information transfer, the crosstalk from "Backward TX" port would not interfere normal forward information transfer.

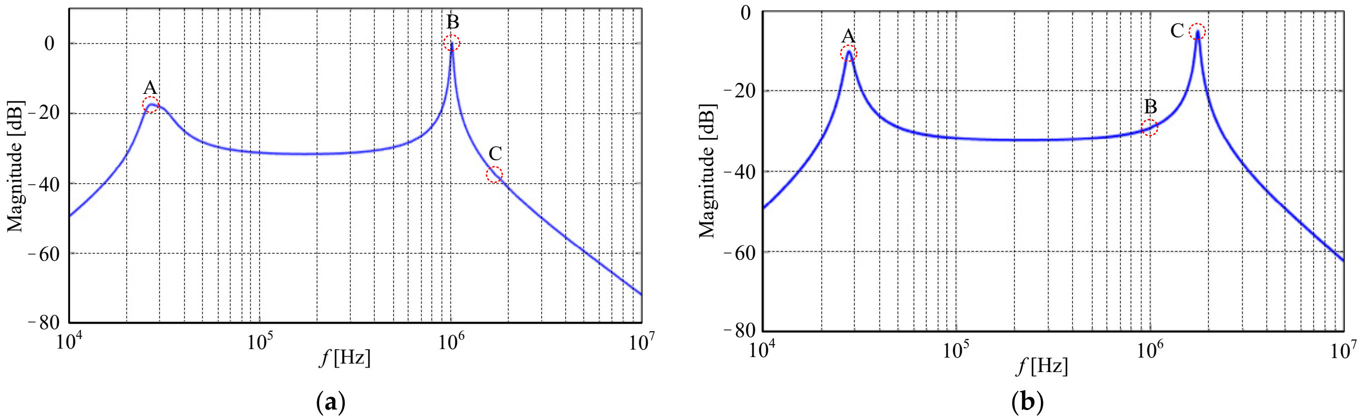

Figure 10. Bode plot of crosstalk interference between forward and backward information transfer. (**a**) Crosstalk from "Backward TX" to "Forward RX". (**b**) Crosstalk from "Forward TX" to "Backward RX".

Similarly, during the backward information transfer, the crosstalk comes from the signal transmitter in the primary side. The gain of the crosstalk $G_{sdc}(\omega)$ is:

$$G_{sdc}(\omega) = \frac{V_{rs}}{V_{dp}} = \frac{Z_{T1}(\omega)}{Z_p(\omega)} \cdot G_{T1}(\omega) \cdot G_{T3}(\omega) \tag{35}$$

The bode of crosstalk $G_{sdc}(\varpi)$ is shown in Figure 10b. There are also only two extreme points. Point A is the power carrier, point B and point C are the information transfer gain in ϖ_{ds} and ϖ_{dp}, respectively. Comparing the gain of $G_{sd}(\varpi_{ds})$ and $G_{sdc}(\varpi_{dp})$, it is clear that $G_{sd}(\varpi_{ds})$ is greater than $G_{sdc}(\varpi_{dp})$. So, during the process of forward information transfer, the crosstalk from "Forward TX" port to "Backward RX" port can be ignored.

In conclusion, normal bidirectional information transmission channels are established in primary and secondary side, but the signal receiving cells in both sides are interfered by the high-frequency source at the same side and the power carrier. According to the models of interference channels and analysis, the coupled coils inductances and self-inductance of tightly coupled transformer affect system efficiency and the gain of information transfer to a certain degree. However, the effect of these crosstalk is limited and does not affect normal information transmission, and then can be ignored.

5. Information Modulation and Demodulation

The previous section analyzes the information transfer channel of the proposed WPT system, which verifies the possibility of full-duplex communication of information. This section introduce signal modulation and demodulation model design.

The schematic in Figure 11a is the structure of information modulation. V_d is the DC voltage source. Q_H and Q_L make up high bridge inverter. C_d is the compensation capacitor. V_T represents a modulated high-frequency voltage source, which is amplified by LC resonance through capacitor C_d and transformer inductor. Through transformer coupling, the high-frequency carrier signal is injected into the power loop through a high-frequency transformer. The receiver circuit in the pick-up side is coincident with the information transmission resonant point to realize the information transmission. After receiving the high-frequency carrier signal, the sampling resistor V_r on the receiving module sends it to the demodulation circuit for signal processing. The structure of demodulation cell is shown in Figure 11b,c.

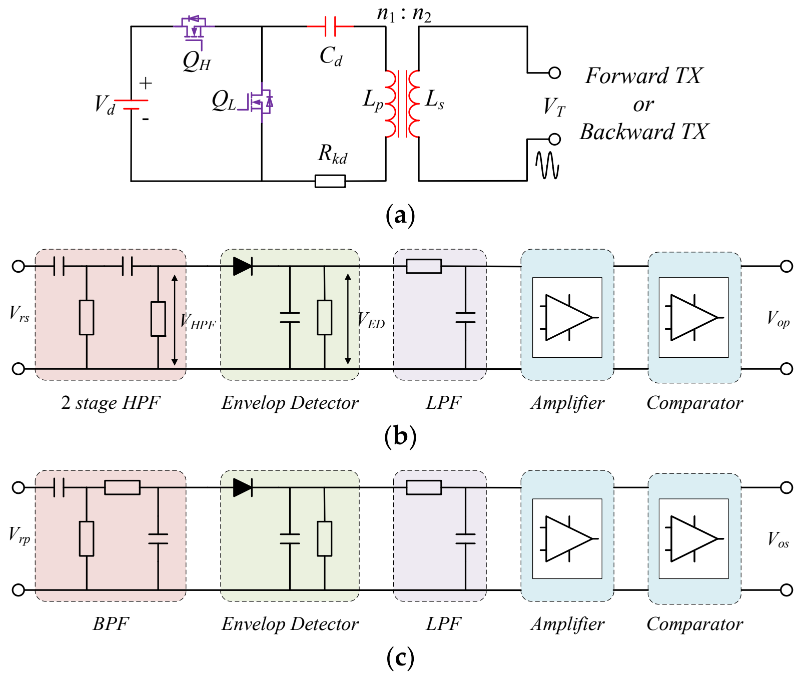

Figure 11. The schematic circuits of modulation and demodulation model. (**a**) Modulation circuit. (**b**) Forward information demodulation circuit. (**c**) Backward information demodulation circuit.

The forward information transmission carrier frequency is set to 1.7 MHz, and the backward transmission carrier is set to 1 MHz. In order to prevent mutual interference between information carriers, the structures of forward and backward information demodulation circuits are different. Therefore, for the forward transmission carrier frequency, the secondary side information demodulation circuit uses a high pass filter (HPF) to filter out the low-frequency power wave and the 1 MHz backward information carrier. And, for backward information transmission, the primary side information processing circuit uses a band-pass filter (BPF), whose band-pass frequencies range from 900 kHz to 1.2 MHz. After passing through the envelop detection (ED) circuit, the voltage peak envelope voltage is obtained. The output waveform is obtained after the signal is sent to the amplifier and comparator circuit.

6. Experimental Verification

To verify the feasibility and effectiveness of the proposed topology and method, a SWIPT system with air gap of 10 cm and 60 W output power is constructed, as shown in Figure 12, The coupling coil disc has a diameter of 8 cm. There are four signal processing boards, two of them are signal transmitting boards, and the other two are signal receiving boards. The system is designed to achieve simultaneous bidirectional transmission of power and data through a shared channel. The system parameters are shown in Table 1.

In order to verify the feasibility of circuit principle and control mode, the current and the voltage in the primary and secondary sides are measured in the process of the experiment. At the same time, for the information transfer, the information transmission at different frequencies and the simultaneous power and information transmission are also measured in the experimental processing, respectively.

In order to verify the impact of the value of α, β and ϕ in this SWIPT system, let $\alpha = 3\pi/4$ and $\beta = 5\pi/6$, ϕ is switched between $-\pi/2$ and $\pi/2$. When V_1 is 48 V, V_2 is 30 V, and the output power is 60 W, Figure 13 shows the voltages and currents of the primary and secondary sides in power transfer loop. Figure 13a displays the power transmitted from the primary side to the secondary side and Figure 13b is the backward power transfer.

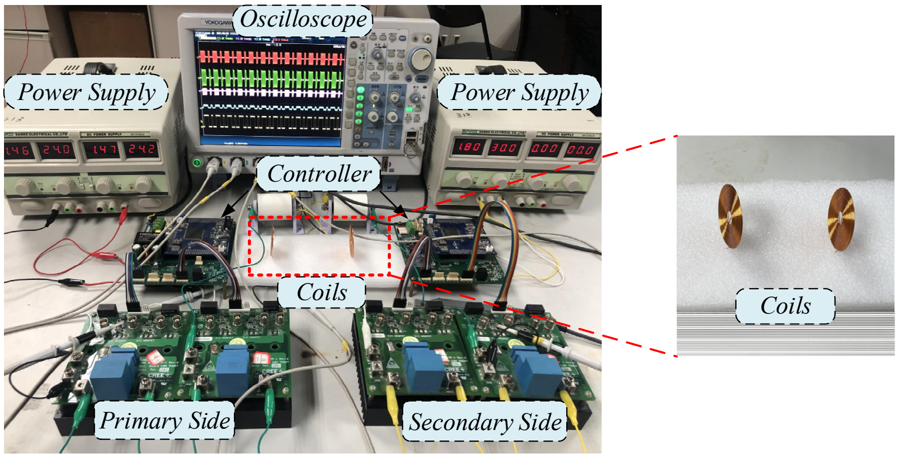

Figure 12. Experimental setup.

Table 1. Parameters of The Proposed WPT System.

Variable	Value	Variable	Value
L_1, L_2	124 µH	L_{T1}~L_{T4}	3 µH
C_1, C_2	250 nF	C_{d1}, C_{d4}	2.2 nF
R_1, R_2	0.05 Ω	C_{d2}, C_{d3}	2.2 nF
f	28.6 kHz	f_{dp}	1.7 MHz
V_1	48 V	f_{ds}	1 MHz
V_2	30 V	d	10 cm
M	36 µH		

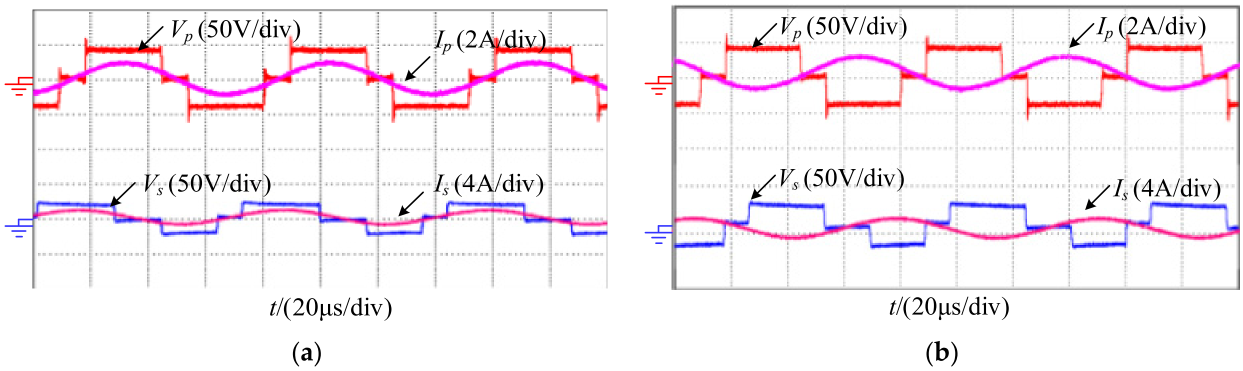

Figure 13. Measured voltage and current waveforms of the primary and the secondary side during bidirectional power transfer. (**a**) Forward power transfer. (**b**) Backward power transfer.

The voltages and the currents are in the same phase. Among them, V_p and V_s are output three-level square wave voltages of the primary side and secondary side. I_p and I_s output the sine wave currents on the primary side and the secondary side, respectively. From Figure 13a,b, it can be seen that the voltage and current are in phase. Therefore, both forward and reverse power transmission are normal. In addition, the operating state of the system is resonant. When $\alpha = \pi$ and $\beta = \pi$, there are only two-level existed in the waveform of V_p and V_s. If $\alpha \neq \pi$ and $\beta \neq \pi$, three-level waveforms appear.

As shown in Figure 14, when the phase shift angle ϕ between the primary and secondary bridge arms changes, the direction of power transmission also changes. When the phase shift angle ϕ between the primary and secondary bridge arms changes from $-\pi/2$

to π/2, the direction of the output current I2 changes too. According to the experimental results, by changing the value of ϕ, the forward transmission of the power is changed to the reverse transmission, that is, the bidirectional transmission is completed, which verifies the previous theoretical analysis.

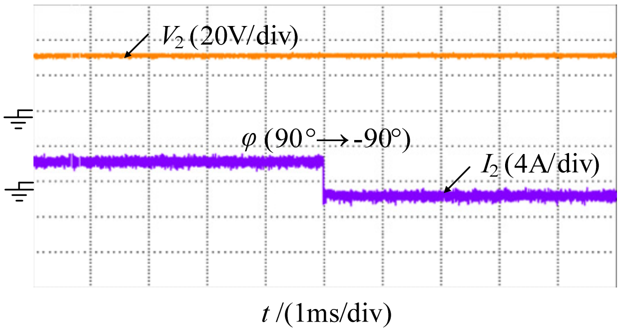

Figure 14. Measured output voltage and current waveforms when the power transmission direction is switched.

Both the information modulation and demodulation cells are connected in series. The full-duplex information transfer adopts frequency shift keying (FSK) control method via a shared channel with power carrier. The signal extracted by the *LC* frequency selection enters the high-pass filter or band-pass filter to remove the influence of the power carrier and other harmonics. After flowing through the detection circuit and the envelope circuit, the signal is sent to the comparator and amplifier circuit. Then, the demodulation module extracts the information encoding. Finally, the information-encoded square waves are obtained.

Figure 15a shows the process of only forward information transferring without power transmission and the communication rate is 20 kbps. V_{T3} is the modulation signal source for the forward information transfer. V_{rs} is the voltage of R_{d2}. V_{HPF} is the output voltage of HPF. After HPF, the low-frequency power waves and other harmonic are filtered out. Then, the envelope detector will follow the peak voltage of V_{HPF} and its output voltage is V_{ENs}. Finally, the forward information transfer signal will be demodulated by amplification and comparison. V_{os} is the output voltage of forward information demodulation cell.

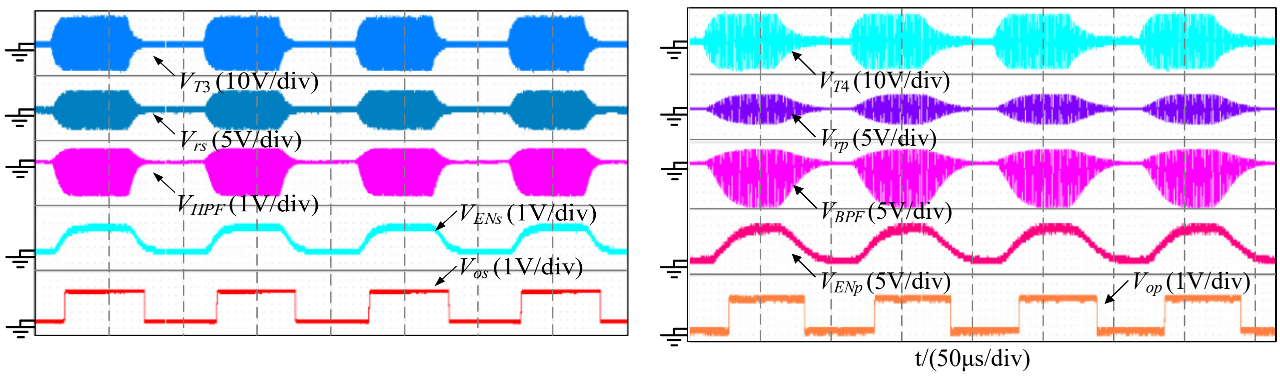

(**a**) (**b**)

Figure 15. The forward and backward information transfer with no power transfer. (**a**) Only forward information transfer. (**b**) Only backward information transfer.

Similarly, the process of only backward information transferring without power transmission is shown in Figure 15b. V_{T4} is the modulation signal source for the backward information transfer. V_{rp} is the voltage of R_{d1}. Contrary to forward information transfer, the structure of demodulation cell for backward information transfer uses BPF to pick up the selected signals. V_{BPF} and V_{ENp} are the output voltage of BPF and envelop detector, respectively. V_{op} is the output voltage of backward information demodulation cell. According to the experimental results, the information transmission is realized correctly.

In Figure 16a,b, the simultaneous wireless information and power transfer is implemented successfully and the communication rate is 20 kbps. The forward and backward information are injected into the power carrier through the modulation signal source in the primary and secondary sides, respectively. Then the waveforms are received at the secondary and primary sides to achieve the demodulation process. Compared with only information transfer, power transmission interferes with the information demodulation, the information can still be received correctly through information demodulation cells.

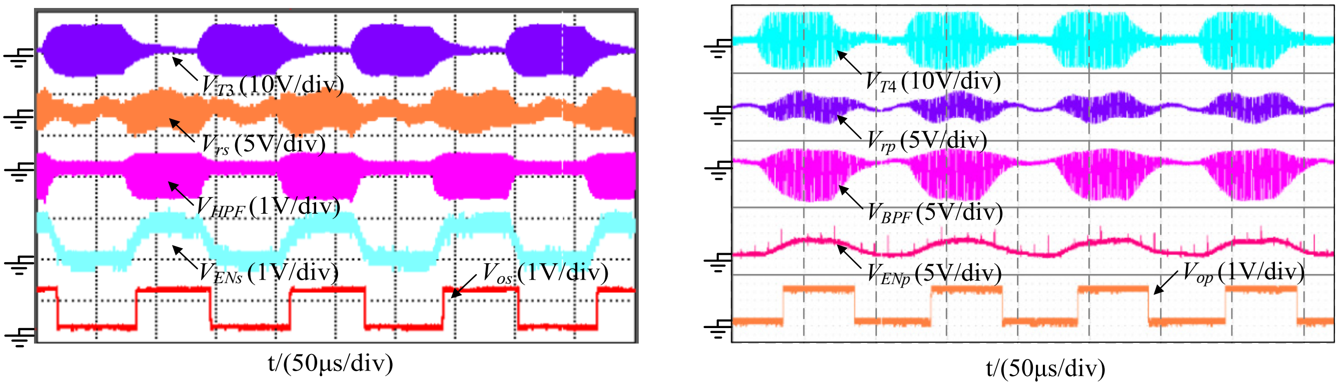

(**a**) (**b**)

Figure 16. The forward and backward information transfer with power transfer. (**a**) Only forward information transfer. (**b**) Only backward information transfer.

Figure 17a presents the process of simultaneous bidirectional information transmission if there is no power carrier in the circuit. V_{T3} and V_{T4} represent the output voltage of tight coupled transformer in primary side and secondary side, respectively. V_{rd} and V_{rs} represent the received high-frequency signal and the filtered information signals, which means the information transmission is completed via a shared channel. V_{op} and V_{os} are the information waveform obtained from the demodulation circuit in both sides.

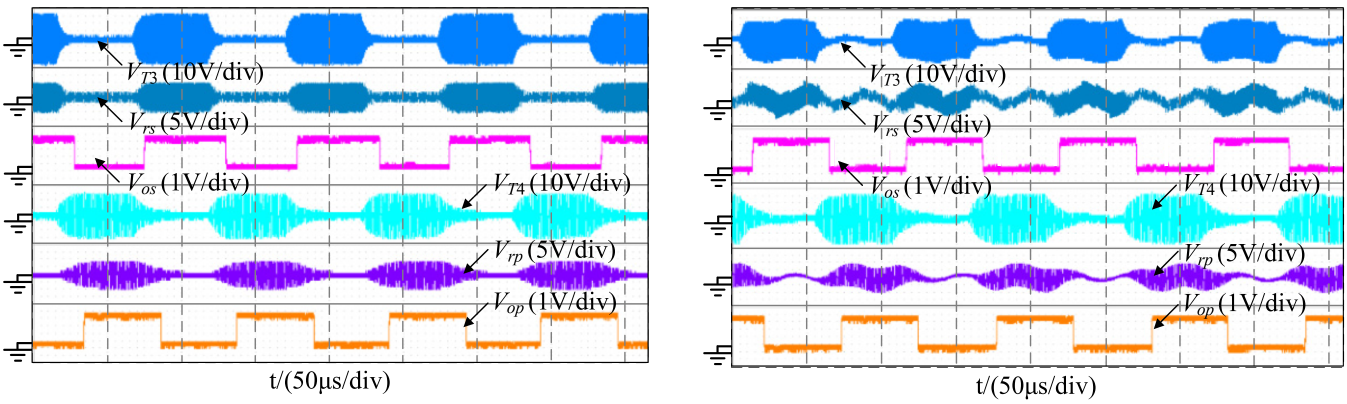

(**a**) (**b**)

Figure 17. The full-duplex communication between the primary side and the secondary side. (**a**) Power carrier does not exist in the circuit. (**b**) Power carrier exists in the circuit.

According to these experimental results, the forward and backward information can be transmitted simultaneously and independently. Similarly, Figure 17b verifies the simultaneous transmission of forward and backward information, the results indicate that information can still be transmitted and demodulated if there is a power carrier in the circuit.

In short, the influence of information carrier on power transmission can be ignored during power transmission; similarly, during information transmission, regardless of power transmission, information can be transferred in full duplex mode.

7. Conclusions

In this paper, a FSK-based SWIPT system with full-duplex communication via a shared channel is established. In this system, the bidirectional power and the full-duplex information transmit at the different frequencies through a shared channel.

When the system is operating, there is a mutual interference between the power transmission channel and the information transmission channel, and between the information channels in the two transmission directions, which brings great difficulties to the analysis of this type of full-duplex SWIPT system.

To solve this problem, this paper proposes an analysis method based on the transmission channel, studies the aforementioned two types of interference problems, and establishes an analysis model for power and information transmission. Experiments show that while there is a relatively complicated mutual interference relationship when the system is running, it can be simplified separately when analyzing power transfer and information transfer. In the experimental prototype, three phase shift control strategy is designed to control the level and direction of output active power. Using the most primitive information transmission method, the full duplex communication rate reaches 20 kbps, and the output active power is 60 W. The experimental results validate the proposed analysis method and model.

Author Contributions: Conceptualization, J.W.; methodology, J.W.; software, P.G.; validation, W.K.; formal analysis, J.W.; investigation, J.Z. and N.J.; resources, J.T. and N.J.; writing—original draft preparation, J.W. and W.K.; writing—review and editing, J.W. and V.S.; supervision, J.W.; project administration, J.W. and V.S.; funding acquisition, J.W. All authors have read and agreed to the published version of the manuscript.

Funding: This work was supported in part by the Scientific and Technological Program of Henan Province under grant 202102210090, 202102210304 and 212102210261.

Data Availability Statement: Not applicable.

Conflicts of Interest: The authors declare no conflict of interest.

References

1. Ramezani, A.; Farhangi, S.; Iman-Eini, H.; Farhangi, B.; Rahimi, R.; Moradi, G.R. Optimized LCC-Series Compensated Resonant Network for Stationary Wireless EV Chargers. *IEEE Trans. Ind. Electron.* **2019**, *66*, 2756–2765. [CrossRef]
2. Babu, A.; George, B. Sensor System to Aid the Vehicle Alignment for Inductive EV Chargers. *IEEE Trans. Ind. Electron.* **2019**, *66*, 7338–7346. [CrossRef]
3. Dai, X.; Jiang, J.; Wu, J. Charging Area Determining and Power Enhancement Method for Multiexcitation Unit Configuration of Wirelessly Dynamic Charging EV System. *IEEE Trans. Ind. Electron.* **2019**, *66*, 4086–4096. [CrossRef]
4. Geng, Y.; Yang, Z.; Lin, F. Design and Control for Catenary Charged Light Rail Vehicle Based on Wireless Power Transfer and Hybrid Energy Storage System. *IEEE Trans. Power Electron.* **2020**, *35*, 7894–7903. [CrossRef]
5. Rizzoli, G.; Mengoni, M.; Tani, A.; Serra, G.; Zarri, L.; Casadei, D. Wireless Power Transfer Using a Five-Phase Wound-Rotor Induction Machine for Speed-Controlled Rotary Platforms. *IEEE Trans. Ind. Electron.* **2020**, *67*, 6237–6247. [CrossRef]
6. Wu, J.; Dai, X.; Gao, R.; Jiang, J. A Coupling Mechanism with Multidegree Freedom for Bidirectional Multistage WPT System. *IEEE Trans. Power Electron.* **2021**, *36*, 1376–1387. [CrossRef]
7. Li, Y.; Hu, J.; Li, X.; Chen, F.; Xu, Q. Analysis, Design, and Experimental Verification of a Mixed High-Order Compensations-Based WPT System with Constant Current Outputs for Driving Multistring LEDs. *IEEE Trans. Ind. Electron.* **2020**, *67*, 203–213. [CrossRef]
8. Song, D.W.; Shi, F.D.; Dai, S.L.; Liu, L. Design and Analysis of a Wireless Power Transmission System with Magnetic Coupling Resonance in Weak-Coupling Region. *Chin. J. Electr. Eng.* **2019**, *5*, 51–60. [CrossRef]
9. Huang, S.Z.; Zhang, J.S.; Wu, W.G.; Xia, L. Impact of Non-Ideal Waveforms on GaN Power FET in Magnetic Resonant Wireless Power Transfer System. *Chin. J. Electr. Eng.* **2019**, *5*, 30–41. [CrossRef]

10. Mude, K.N.; Aditya, K. Comprehensive Review and Analysis of Two Element Resonant Compensation Topologies for Wireless Inductive Power Transfer Systems. *Chin. J. Electr. Eng.* **2019**, *2*, 14–31. [CrossRef]
11. Wu, L.H.; Zhang, B. Reconfigurable Transmitter Coil Structure for Highly Efficient and Misalignment-Insensitive Wireless Power Transfer Systems in Megahertz Range. *Chin. J. Electr. Eng.* **2019**, *2*, 56–62. [CrossRef]
12. Singh, J.; Tiwari, R. Cost Benefit Analysis for V2G Implementation of Electric Vehicles in Distribution System. *IEEE Trans. Ind. Appl.* **2020**, *56*, 5963–5973. [CrossRef]
13. Chung, Y.D.; Park, E.Y.; Lee, W.S.; Lee, J.Y. Impact Investigations and Characteristics by Strong Electromagnetic Field of Wireless Power Charging System for Electric Vehicle Under Air and Water Exposure Indexes. *IEEE Trans. Appl. Supercon.* **2018**, *28*, 1–5. [CrossRef]
14. Li, Y.; Lin, T.; Mai, R.; Huang, L.; He, Z. Compact Double-Sided Decoupled Coils-Based WPT Systems for High-Power Applications: Analysis, Design, and Experimental Verification. *IEEE Trans. Transp. Electrif.* **2018**, *4*, 64–75. [CrossRef]
15. Wu, J.; Zhang, H.Y.; Gao, P.F.; Dou, Z.F.; Jin, N.; Snasel, V. Dual-Frequency Programmed Harmonics Modulation-based Simultaneous Wireless Information and Power Transfer System via a Common Resonance Link. *Sustainability* **2020**, *12*, 4189. [CrossRef]
16. Varshney, L.R. Transporting information and energy simultaneously. In Proceedings of the 2008 IEEE International Symposium on Information Theory, Toronto, ON, Canada, 6–11 July 2008; pp. 1612–1616.
17. Grover, P.; Sahai, A. Shannon meets Tesla: Wireless information and power transfer. In Proceedings of the 2010 IEEE International Symposium on Information Theory, Austin, TX, USA, 13–18 June 2010; pp. 2363–2367.
18. Clerckx, B.; Zhang, R.; Schober, R.; Ng, D.W.K.; Kim, D.I.; Poor, H.V. Fundamentals of Wireless Information and Power Transfer: From RF Energy Harvester Models to Signal and System Designs. *IEEE J. Sel. Areas Commun.* **2018**, *37*, 4–33. [CrossRef]
19. Ma, R.; Wu, H.; Ou, J.; Yang, S.; Gao, Y. Power Splitting-Based SWIPT Systems with Full-Duplex Jamming. *IEEE Trans. Veh. Technol.* **2020**, *69*, 9822–9836. [CrossRef]
20. Choi, K.W.; Hwang, S.I.; Aziz, A.A.; Jang, H.H.; Kim, J.S.; Kang, D.S.; Kim, D.I. Simultaneous Wireless Information and Power Transfer (SWIPT) for Internet of Things: Novel Receiver Design and Experimental Validation. *IEEE Internet Things J.* **2020**, *7*, 2996–3012. [CrossRef]
21. Rajaram, A.N.D.; Jayakody, K.; Chen, B.; Dinis, R.; Affes, S. Modulation-Based Simultaneous Wireless Information and Power Transfer. *IEEE Commun. Lett.* **2020**, *24*, 136–140. [CrossRef]
22. He, S.; Tang, Y.; Li, Z.; Li, F.; Xie, K.; Kim, H.; Kim, G. Interference-Aware Routing for Difficult Wireless Sensor Network Environment with SWIPT. *Sensors* **2019**, *19*, 3978. [CrossRef] [PubMed]
23. Wu, J.; Zhao, C.Y.; Jin, N.; He, S.B.; Ma, D.G. Bidirectional Information Transmission in SWIPT System with Single Controlled Chopper Receiver. *Electronics* **2019**, *8*, 1027. [CrossRef]
24. Yu, C.; Lu, R.; Su, C.; Zhu, C. Study on Wireless Energy and Data Transfer for Long-Range Projectile. *IEEE Trans. Plasma Sci.* **2013**, *41*, 1370–1375.
25. Shirichian, M.; Chamaani, S.; Akbarpour, A.; Galdo, G.D. Analysis and Design of Broadband Simultaneous Wireless Information and Power Transfer (SWIPT) System Considering Rectifier Effect. *Energies* **2018**, *11*, 2387. [CrossRef]
26. Li, X.; Hu, J.; Li, L.; Wang, H.; Liu, M.; Deng, P. A Decoupled Power and Data-Parallel Transmission Method with Four-Quadrant Misalignment Tolerance for Wireless Power Transfer Systems. *IEEE Trans. Power Electron.* **2019**, *34*, 11531–11535. [CrossRef]
27. Ji, L.; Wang, L.; Liao, C.; Li, S. Simultaneous Wireless Power and Bidirectional Information Transmission with a Single-Coil, Dual-Resonant Structure. *IEEE Trans. Ind. Electron.* **2019**, *66*, 4013–4022. [CrossRef]
28. Peng, K.; Tang, X.; Mai, S.; Wang, Z. A Simultaneous Power and Downlink Data Transfer System with Pulse Phase Modulation. *IEEE Trans. Circuits Syst. II Express Briefs* **2019**, *66*, 808–812. [CrossRef]
29. Lee, H.; Kim, J.; Ha, D.; Kim, T.; Kim, S. Differentiating ASK Demodulator for Contactless Smart Cards Supporting VHBR. *IEEE Trans. Circuits-II* **2015**, *62*, 641–645. [CrossRef]
30. Huang, C.; Lin, C. Wireless Power and Bidirectional Data Transfer Scheme for Battery Charger. *IEEE Trans. Power Electron.* **2018**, *33*, 4679–4689. [CrossRef]
31. Kim, J.; Wei, G.; Kim, M.; Ryo, H.; Zhu, C. A Wireless Power and Information Simultaneous Transfer Technology Based on 2FSK Modulation Using the Dual Bands of Series–Parallel Combined Resonant Circuit. *IEEE Trans. Power Electron.* **2019**, *34*, 2956–2965. [CrossRef]
32. Liu, L.; Ding, Z.; Elkashlan, M.; Poor, H. Cooperative Non -orthogonal Multiple Access with Simultaneous Wireless Information and Power Transfer. *IEEE J. Sel. Areas Commun.* **2016**, *34*, 938–953. [CrossRef]
33. Wu, J.; Zhao, C.; Lin, Z.; Du, J.; Hu, Y.; He, X. Wireless Power and Data Transfer via a Common Inductive Link Using Frequency Division Multiplexing. *IEEE Trans. Ind. Electron.* **2015**, *62*, 7810–7820. [CrossRef]
34. Yao, Y.; Wang, Y.; Liu, X.; Cheng, H.; Liu, M.; Xu, D. Analysis, Design, and Implementation of a Wireless Power and Data Transmission System Using Capacitive Coupling and Double-Sided LCC Compensation Topology. *IEEE Trans. Ind. Appl.* **2019**, *55*, 541–551. [CrossRef]
35. Qian, Z.; Yan, R.; Wu, J.; He, X. Full-Duplex High-Speed Simultaneous Communication Technology for Wireless EV Charging. *IEEE Trans. Power Electron.* **2019**, *34*, 9369–9373. [CrossRef]
36. Yao, Y.; Cheng, H.; Wang, Y.; Mai, J.; Lu, K.; Xu, D. An FDM-Based Simultaneous Wireless Power and Data Transfer System Functioning with High-Rate Full-Duplex Communication. *IEEE Trans. Ind. Inform.* **2020**, *16*, 6370–6381. [CrossRef]